AIAA JOURNAL
Vol. 47, No. 1, January 2009

Evaluation of Euler Fluxes for Hypersonic Flow Computations

Keiichi Kitamura*
Japan Aerospace Exploration Agency, Sagamihara 229-8510, Japan
Philip Roe†
University of Michigan, Ann Arbor, Michigan 48109-2140
and
Farzad Ismail‡
University of Iowa, Iowa City, Iowa 52242-1585

DOI: 10.2514/1.33735

Shock-capturing finite volume schemes often give rise to anomalous results in hypersonic flow. We present a wide-ranging survey of numerical experiments from 12 different flux functions in one- and two-dimensional contexts. Included is a recently developed function that satisfies the second law of thermodynamics. It is found here that there are at least two kinds of shock instabilities: one is one-dimensional and the other is multidimensional. According to the results, the former does not appear if a flux function satisfies the second law of thermodynamics, and the latter is suppressed by an additional dissipation with a multidimensional character. However, such dissipation has no effect on the one-dimensional mode. Among the flux functions investigated, no universally stable schemes are found that are free from both one- and multidimensional shock instabilities. The appearance of these instabilities depends on the relative positioning of the shock on the grid.

Nomenclature

e	=	internal energy, $(p/\rho)/(\gamma\text{-}1)$
e_t	=	total energy, $e + (1/2)(u^2 + v^2)$
H	=	total enthalpy, $e_t + p/\rho$
i, j	=	cell indices
M	=	Mach number
p	=	pressure
S	=	entropy, $\ln p - \gamma \ln \rho$
u, v	=	velocity components
x, y	=	Cartesian coordinates
α	=	entropy coefficient in the entropy-consistent Roe scheme
γ	=	specific heat ratio, 1.4
δ	=	grid-stretch parameter, $0, 1/8, \ldots, 1$
ε	=	shock-position parameter, $0.0, 0.1, \ldots, 0.9$
ρ	=	density

Subscripts

L	=	left state (prestate) of the shock
M	=	intermediate state (internal state) of the shock
R	=	right state (poststate) of the shock
0	=	freestream value

I. Introduction

THE computation of hypersonic flows has proved surprisingly troublesome on account of anomalies, such as carbuncle phenomenon [1], which afflicts shock-capturing schemes. The carbuncle phenomenon appears to be very complex [2], but theoretical discussion is hampered by the fact that the carbuncle is a real physical solution and so cannot be excluded by the application of any simple physical principle. We feel convinced that there is no single cause, nor is there any single cure. Several schemes have been published with claims that they do not suffer from such effects. However, it is difficult to establish such claims theoretically, because we still lack an accepted explanation for the breakdowns. It is also difficult to establish them experimentally, because the phenomena depend on many factors (e.g., mesh geometry, mesh size, flow Mach number, and specific heat ratio) [2,3]. In this paper, we pursue an experimental comparison from a viewpoint that is partly physical and partly numerical. We will pay particular attention to those schemes known to fail [4,5] and to schemes specifically claimed to avoid the phenomenon [6–10]. Also, we will focus on a recently published method [11–14] that is an entropy-consistent development of the Roe scheme.

We have organized our investigation as follows around the hypothesis that part of the mechanism for generating the carbuncle is one-dimensional (1-D) and part is multidimensional:

1) In the 1-D problem, we begin by analyzing the apparently trivial problem of a steady shock in one dimension. The parameter here is the shock location on the grid and the flow Mach number.

2) In the 1-1/2-D problem, our next experiments are what we refer to as 1-1/2-dimensional, in which we simply stack identical 1-D problems on top of each other to form a two-dimensional (2-D) mesh of squares. The parameter here is the shock location, and the objective is to see whether the same outcome can be drawn as in the previous test. Several authors have proposed fluxes that are intended to cure the carbuncle by an additional dissipation term with a multidimensional character. It is also investigated whether such terms are effective in cure for the shock instabilities.

3) In the 2-D problem, as a more practical test, we consider the flow past a circular cylinder, using a grid in which one mesh line (set of cell interfaces) coincides with the shock obtained from a shock-fitting code. Naively, one might expect that mesh alignment of this kind would make it easy to capture the shock, but the 1-1/2-D test refutes this expectation. We made a series of tests in which the mesh was progressively dilated until, near the shock, the mesh lines were displaced by precisely one cell width. Thus, the shock took up all possible locations relative to the grid line, just as in the previous experiments.

According to the results, 1-D and multidimensional effects in shock instabilities are discussed separately, and more insight in these

Presented as Paper 4465 at the 18th AIAA Computational Fluid Dynamics Conference, Miami, FL, 25–28 June 2007; received 28 July 2007; revision received 23 September 2008; accepted for publication 2 July 2008.

*Researcher, Engineering Digital Innovation Center; kitamura.keiichi@jaxa.jp. Member AIAA.
†Professor, Department of Aerospace Engineering. Fellow AIAA.
‡Postdoctoral Associate, Iowa Institute of Hydraulic Research, Hydroscience and Engineering. Member AIAA.

instabilities will be explored. A final remark for developing a reliable flux function will follow.

II. Numerical Methods

A. Governing Equations

The governing equations are two-dimensional compressible Euler equations as follows:

$$\frac{\partial \mathbf{u}}{\partial t} + \frac{\partial \mathbf{F}}{\partial x} + \frac{\partial \mathbf{G}}{\partial y} = 0 \tag{1a}$$

$$\mathbf{u} = \begin{bmatrix} \rho \\ \rho u \\ \rho v \\ \rho e_t \end{bmatrix}, \qquad \mathbf{F} = \begin{bmatrix} \rho u \\ \rho u^2 + p \\ \rho uv \\ \rho uH \end{bmatrix}, \qquad \mathbf{G} = \begin{bmatrix} \rho v \\ \rho vu \\ \rho v^2 + p \\ \rho vH \end{bmatrix} \tag{1b}$$

where ρ is density, u and v are velocity components in Cartesian coordinates, p is pressure, e_t is total energy, and H is total enthalpy ($H = e_t + p/\rho$). The calorically-perfect-gas model is assumed for air with the specific heat ratio $\gamma = 1.4$. These equations are solved by the finite volume method. Both the spatial and the time accuracies are first order if not mentioned otherwise. As for the numerical flux at each cell interface, 12 different functions are used, including a recently published entropy-consistent (EC) Roe scheme. A brief introduction for this scheme appears in the next subsection.

B. Entropy-Stable and Entropy-Consistent Schemes

The new *entropy-stable* scheme is described in [11–14]. Basically, the standard formula

$$\mathbf{F}^* = \mathbf{F} - \tfrac{1}{2}\mathbf{R}|\hat{\mathbf{\Lambda}}|\mathbf{L}\,\mathbf{\Delta u} \tag{2}$$

is replaced by

$$\mathbf{F}^* = \mathbf{F}_c - \tfrac{1}{2}\mathbf{R}|\hat{\mathbf{\Lambda}}\,\hat{\mathbf{S}}\,|\mathbf{R}^{\mathbf{T}}\mathbf{\Delta v} \tag{3a}$$

where $\mathbf{F}_C$ is a special averaging ($\hat{}$) of the left and right states that conserves entropy,

$$\mathbf{F}_c = [\hat{\rho}\,\hat{u}, \hat{\rho}\hat{u}^2 + \hat{p}_1, \hat{\rho}\,\hat{u}\,\hat{v}, \hat{\rho}\,\hat{u}\,\hat{H}]^{\mathbf{T}} \tag{3b}$$

$\mathbf{S}$ is a scaling factor,

$$\mathbf{S} = \mathrm{diag}\left(\frac{\hat{\rho}}{2\gamma}, \frac{(\gamma-1)\hat{\rho}}{\gamma}, \hat{p}_1, \frac{\hat{\rho}}{2\gamma}\right) \tag{3c}$$

and the dissipation term is not driven by the jump $\mathbf{\Delta u}$ in the conserved variables, but by the jump $\mathbf{\Delta v}$ in the entropy variables:

$$\Delta\mathbf{v} = \left[\Delta\left(\frac{\gamma - S}{\gamma - 1} - \frac{\rho(u^2+v^2)}{2p}\right), \Delta\left(\frac{\rho u}{p}\right), \Delta\left(\frac{\rho v}{p}\right), -\Delta\left(\frac{\rho}{p}\right)\right]^{\mathbf{T}} \tag{3d}$$

The diagonal matrix of eigenvalues is replaced by $|\hat{\mathbf{\Lambda}}| \to |\hat{\mathbf{\Lambda}}| + \alpha|\Delta\mathbf{\Lambda}|$, where the additional term $\alpha|\Delta\mathbf{\Lambda}|$ is introduced to ensure that the entropy produced by a shock is of third order, as it should be. The coefficient alpha is not rigorously derived. For a weak shock sharply resolved, it should be $1/6$. For stronger or less-well-resolved shocks, it needs to be larger, and we are presently engaged in trying to make this more precise ($\alpha = 0.2$ or 0.8 in the present paper). This *entropy-consistent* scheme is called the *EC-Roe scheme* in this paper. Because the analysis on which it is based is only semidiscrete, we have employed a small Courant–Friedrichs–Lewy (CFL) number when applying this scheme (see Table 1).

Table 1 CFL number chosen for each freestream Mach number M_0

M_0	1.5–6.0	10.0	20.0
CFL	0.5	0.2	0.1

III. Numerical Experiments

A. One-Dimensional Problem: Steady Normal Shock

From the viewpoint of continuum mechanics, a shock wave is regarded as a thin jump discontinuity, but a captured shock has numerical internal structure. However, it is hard to establish what this internal structure should be [3,15,16]. For example, the Godunov and Roe schemes produce an intermediate state that lies on the Hugoniot curve joining $\mathbf{u}_R$ to $\mathbf{u}_L$, but such a state does not preserve mass flux inside the shock. On the other hand, at least one intermediate state is needed to allow representation of a shock that is not precisely located at a mesh interface. Therefore, we prescribe initial conditions that include an intermediate state and boundary conditions that force the shock to remain in its initial position. The grid comprises 50 equally spaced cells, as in Fig. 1, with initial conditions for left (L: $i \le 12$) and right (R: $i \ge 14$):

$$\mathbf{u}_L = \begin{bmatrix} 1 \\ 1 \\ 0 \\ \frac{1}{\gamma(\gamma-1)M_0^2} + \frac{1}{2} \end{bmatrix}, \qquad \mathbf{u}_R = \begin{bmatrix} f(M_0) \\ 1 \\ 0 \\ \frac{g(M_0)}{\gamma(\gamma-1)M_0^2} + \frac{1}{2f(M_0)} \end{bmatrix} \tag{4a}$$

where

$$f(M_0) = \left(\frac{2}{(\gamma+1)M_0^2} + \frac{\gamma-1}{\gamma+1}\right)^{-1}, \qquad g(M_0) = \frac{2\gamma M_0^2}{\gamma+1} - \frac{\gamma-1}{\gamma+1} \tag{4b}$$

following the Rankine–Hugoniot conditions across the normal shock. The internal shock conditions (M: $i = 13$) are as follows:

1) The density is given as

$$\rho_M = \varepsilon\rho_L + (1\text{-}\varepsilon)\rho_R \tag{5}$$

where the shock-position parameter $\varepsilon = 0.0, 0.1, \ldots, 0.9$.

2) The other variables are calculated based on ρ_M so that all variables lie on the Hugoniot curve, connected to $\mathbf{u}_L$ and $\mathbf{u}_R$, as in [16].[§]

At the outflow boundary, we prescribe the mass flux at the ghost cell ($i = i_{\max} + 1$)

$$(\rho u)_{i\max+1,j} = (\rho u)_0 = 1 \tag{6}$$

for the mass in the whole computational domain to remain constant and for the shock to be fixed at the same position; meanwhile, other values are simply extrapolated (e.g., $\rho_{i\max+1,j} = \rho_{i\max,j}$). In other words, this set of the outflow boundary conditions mimics the situation in which a normal shock sits in front of a wall constantly. (Under the standard wall condition, the shock goes upstream, of course, until it reaches the inflow boundary. If another outflow

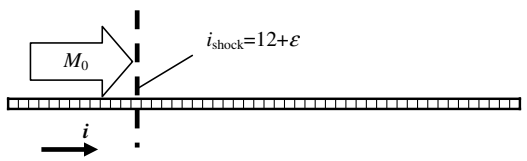

Fig. 1 Computational grid and conditions for the 1-D steady shock test problem.

[§]Though there are some alternative ways to determine internal shock states [e.g., all the primitive variables can be given as $\mathbf{u}_M = \varepsilon\mathbf{u}_L + (1\text{-}\varepsilon)\mathbf{u}_R$], we confirmed that these have minor effects on our conclusions.

condition is applied, the outflow boundary no longer behaves as the wall and different results are obtained.[¶])

The inflow boundary has the freestream values. The freestream Mach number is chosen in the range $1.5 \leq M_0 \leq 20.0$. If a scheme is always stable for all those values of ε and M_0, the scheme can be labeled as 1-D stable.

Then the computations are conducted until when time steps multiplied by the CFL number reached 20,000 (e.g., 100,000 steps with CFL $= 0.2$), and the CFL number is chosen depending on M_0, as in Table 1, based on stability limit of the EC-Roe scheme [11]. To see how well upwind schemes preserve the initial shock position, we compare results of the following widely used or recently proposed schemes, such as Godunov's exact Riemann solver [4]; Roe's (original) scheme [5], which is a linear approximate Riemann solver; Roe scheme with Harten's entropy fix (E-fix) [17], which removes expansion shock; AUSM+ [6], AUSM$^+$-up [7], AUSMPW+ [8] and RoeM2 [9] schemes, which preserve total enthalpy H in steady flow; and HLLE [10], which is widely believed to be a carbuncle-free but notoriously dissipative scheme.

The behaviors of those schemes are summarized in Fig. 2. If the L2-norm of density residual dropped at least 3 orders of magnitude, the computation is stable (O in the figure). If, on the other hand, the shock was moving back and forth and the computation did not converge, it is unstable ($\times$ in the figure). These typical solutions are shown in Fig. 3. In stable cases, the contours are identical from 10,000 (not shown) through 50,000 steps, but not in the unstable cases, as the shock is still moving.

The following can be seen from Fig. 2:

1) The Roe scheme with E-fix and the EC-Roe scheme with a large entropy-coefficient ($\alpha = 0.8$) are 1-D stable in all cases, whereas others are not. The other schemes are stable only for low Mach numbers ($M_0 < 2.0$, except for AUSM+ and AUSM$^+$-up schemes) or for particular shock positions, depending on the schemes. Thus, most schemes that are claimed as carbuncle-free are actually not stable in a 1-D calculation. This aspect of the carbuncle has been largely ignored by researchers, but our contention is that one-dimensional stability is crucial for curing the carbuncle. In the following subsections, we will extend this discussion to two-dimensional problems. We also point out here that those two successful fluxes can resolve shear/boundary-layers well, as reported in [11,18,19].

2) The shock location ϵ for the unstable results are generally different for different schemes. However, the results for the exact (Godunov) Riemann solver and the unmodified Roe scheme are almost identical, as pointed out by Barth [3]. According to the present criterion which divides stable and unstable cases, only one exception is seen at $M_0 = 4.0$ and $\varepsilon = 0.7$. In addition, these solutions for $\varepsilon = 0.0$ are not necessarily stable under the current setup, in which the downstream boundary plays a significant role, though the two Riemann solvers were designed to accurately capture the shock when it properly sits on the mesh line.

B. One-and-One-Half-Dimensional Problem: Steady Normal Shock

Next we solved a steady shock that is initially aligned in one direction in a 2-D field (Fig. 4). We expect that such a computed flowfield should behave in a 1-D manner unless multidimensional instability is introduced, and thus we call this problem a 1-1/2-D problem. This is a simplified carbuncle problem that was developed first by Quirk [20] and modified by Dumbser et al. [21], but we used a grid that is extended farther downstream from the shock. We found that this made the development of unstable solutions more likely. In particular, we employed a grid with 50×25 cells spaced evenly without any perturbation (no other kinds of perturbations are introduced either). The freestream Mach number chosen is $M_0 = 6.0$, because the solutions in the 1-D problem are almost the same for $M_0 \geq 6.0$ (Fig. 2). The periodical condition is imposed for the boundaries of j direction, whereas the other initial conditions and boundary conditions are the same as in the 1-D tests. The computations were conducted for 40,000 steps with CFL $= 0.5$. If a scheme is stable for all the shock positions ε, the scheme can be labeled as 1-1/2-D stable.

Our computations are summarized in Table 2, showing a comparison with 1-D results. In this table, the following notations are used:

1) S denotes a case in which the code converged steadily and exponentially toward a satisfactory solution.

2) U denotes a case in which the residual hung up at some stage and the solution remained of poor quality. This case resembles 1-D unstable or a carbuncle solution.

3) A denotes a case similar to U, but in which the residual eventually began to decrease again, with convergence to an unsatisfactory solution, usually asymmetric and in the form of a carbuncle.

As can be seen, there is no 1-1/2-D stable scheme. Overall, the case that was stable in 1-D was more likely to be 1-1/2-D stable than the 1-D unstable case, and almost no case that was unstable in 1-D proved to be stable in 1-1/2-D (with few exceptions). In addition, if there are both 1-D and 1-1/2-D stable cases and 1-D and 1-1/2-D unstable/asymmetric cases, these cases are sometimes separated by 1-D stable but 1-1/2-D unstable/asymmetric (or vice versa) cases. Therefore, we claim that 1-D stability is crucial for 1-1/2-D stability.

1. *Shock Locations that are Stable in One Dimension*

Here, we show only cases that were stable in 1-D. In Fig. 5, Mach number contours at 40,000 time steps are shown for typical cases, and Fig. 6 shows representative profiles of the L2-norm of density residual histories for these calculations. The tests reported in this subsection determine how the 1-1/2-D instability develops. The instabilities that appeared sometimes took the form of local oscillations confined to the shock [stage 1 (Fig. 5d)], streaks of vorticity streaming behind the shock [stage 2 (Fig. 5e)] or total breakdown [stage 3 (Figs. 5f and 5g)] [11,22]. In the last case, the density behind the shock is no longer that behind a normal shock, and even under our new boundary condition, the shock is free to move and may eventually disappear off the grid (Fig. 5h). In this case, the residual suddenly drops to the machine-zero level when the shock is wiped out (Fig. 6b). The following features of these results are noteworthy from Table 2 and Figs. 5 and 6:

1) The only two schemes that were universally stable in 1-D (the EC-Roe scheme with $\alpha = 0.8$ and Roe's scheme with Harten's E-fix) both failed this test. Thus, it is found that there is 1-1/2-D stability that is distinct from 1-D stability. Moreover, many of the schemes that were stable in 1-D for some particular combination of M_0 and ε are unstable here. Hence, 1-D stability is not sufficient for the 1-1/2-D stability.

2) Comparing the results of the EC-Roe scheme with $\alpha = 0.2$ and 0.8, we can see that the latter is more unstable than the former in this test, in contrast to 1-D tests. Thus, although adding dissipation in a direction normal to a shock enhances 1-D stability, we think another strategy has to be considered for a direction parallel to the shock to establish a 1-1/2-D stable scheme. This also holds for a comparison of the original Roe and Roe (E-fix).

3) The AUSM+ solution has a surprising feature when $\varepsilon = 0.7$: after the residual once converged to $\mathcal{O}(10^{-11})$ with an apparently stable solution (shown in Fig. 7a), the flowfield suddenly destabilized around 10,000 steps. Then the residual grew exponentially and remained at a significant magnitude (Fig. 6c). Eventually, the calculation reached the stage 1 carbuncle solution [20,000 steps (Fig. 7b) and 40,000 steps (Fig. 5d)]. Further explanation will appear later; this scheme cannot be called 1-1/2-D stable.

4) The AUSM$^+$-up scheme showed the stage 2 carbuncle solution for $\varepsilon = 0.8$ (Fig. 5e), and the residual stagnated at around $\mathcal{O}(10^{-5})$ (not shown). This scheme, again, is not 1-1/2-D stable.

5) The AUSMPW+ scheme has a multidimensional term and is claimed to be carbuncle-free. With this term, as can be expected, the results were stable whenever the 1-D case was stable (Table 2).

[¶]Private communication with Tomoyuki Hanawa, Chiba University, Japan, Nov. 2007.

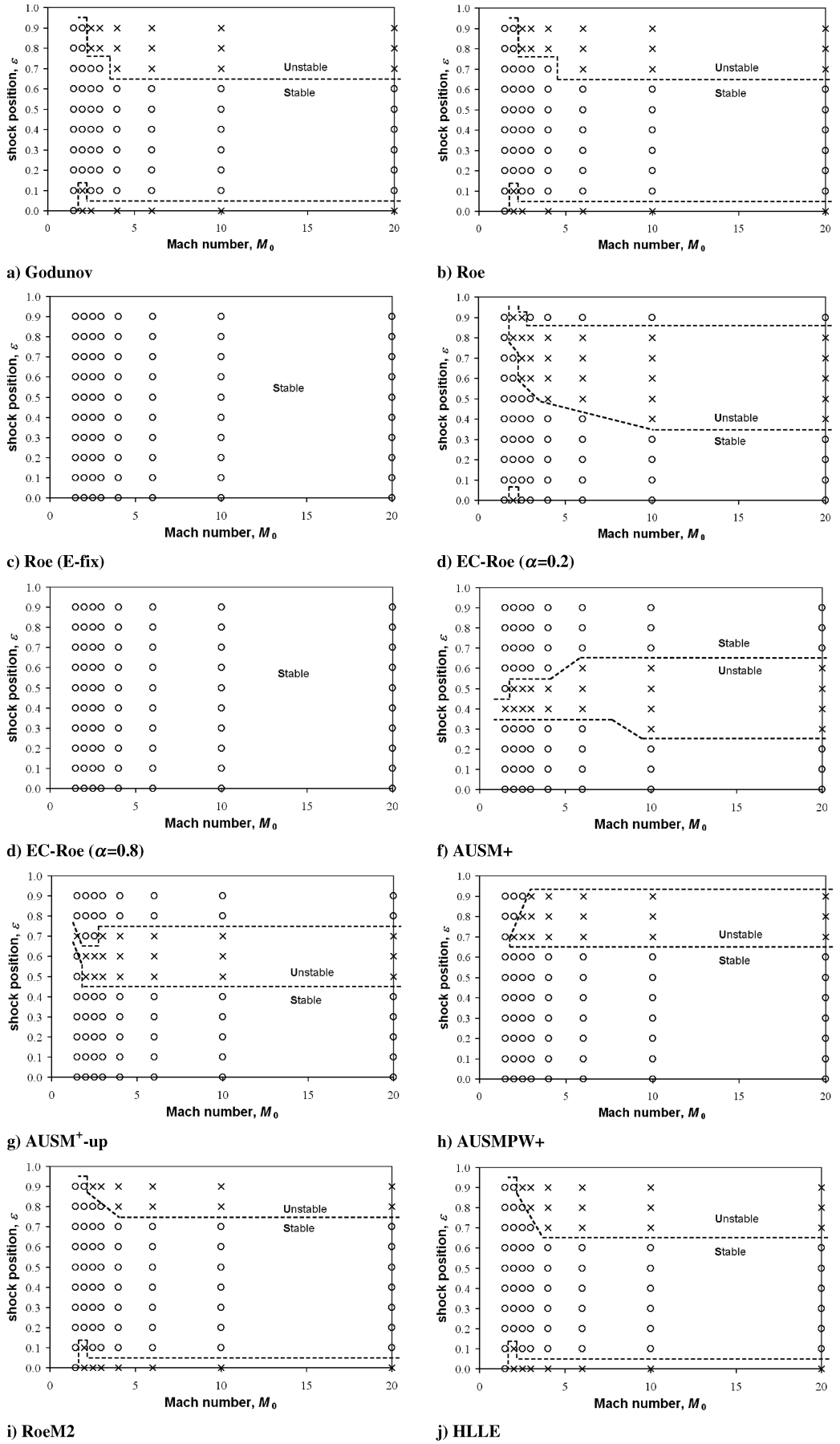

Fig. 2 One-dimensional stability limits for upwind schemes (freestream Mach number $1.5 \le M_0 \le 20.0$ and shock position $\varepsilon = 0.0, 0.1, \ldots, 0.9$).

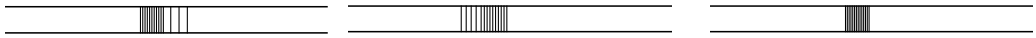

a) Stable (Roe, ε=0.5, 50,000 steps) b) Unstable (Roe, ε=0.0, 49,000 steps) c) Unstable (Roe, ε=0.0, 50,000 steps)

Fig. 3 Typical examples of Mach number contours for the 1-D steady shock (freestream Mach number $M_0 = 2.0$).

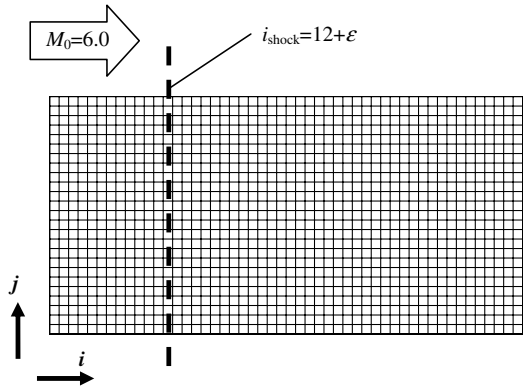

Fig. 4 Computational grid and conditions for 1-1/2-D steady shock test problem.

However, when that multidimensional term was eliminated, the solutions did not converge in some cases (e.g., $\varepsilon = 0.0, 0.5$, and 0.6). Hence, the multidimensional term properly works as is designed.

6) The RoeM2 scheme also has a multidimensional term and is claimed to be carbuncle-free. With this term, in contrast to AUSMPW+, the results were either stable or unstable when the 1-D case was stable (Table 2 and Fig. 5c). When the multidimensional term was eliminated, the solutions were either stabilized or destabilized, depending on ε (Table 2). This may be attributed to the aforementioned fact that too much dissipation addition to the direction parallel to the shock can lead to unstable solutions. Moreover, with a multidimensional term for $\varepsilon = 0.5$, the solution was once destabilized around 24,000 steps, similarly to AUSM+ ($\varepsilon = 0.7$), but in this case, the solution remained stable (according to the present criteria) for 200,000 steps (shown in Fig. 8).

7) The HLLE scheme, the only scheme known to be carbuncle-free among widely used schemes (though it lacks resolution of contact discontinuities and boundary layers), showed a stable result whenever the 1-D case was stable.

In search of more insight, we measured how the unstable 1-1/2-D solutions deviated from the stable 1-D solutions; specifically, we computed the L1-norm of differences of the primitive variables (ρ, u, v, p). Figure 9 shows the time histories of the deviations from the 1-D solutions for selected results (only u and v are shown, for brevity, because ρ and p behaved as the same manner as u). The deviation of v stands for the amount of 1-1/2-D instability. A noteworthy conclusion is that in all of the unstable cases except two, the deviation grew rapidly and immediately in all variables (e.g., Figs. 9b and 9c). The exceptions were AUSM+ [$\varepsilon = 0.7$ (Fig. 9e)] and RoeM2 [$\varepsilon = 0.5$ (Fig. 8c)], for which the growth was very gentle. This accounts for the apparently satisfactory stability of these schemes at early times; that is, the 1-D instability did not appear and the solution went toward the convergence, whereas the 1-1/2-D instability subliminally grew. Thus, one should pay careful attention when applying AUSM+ or RoeM2 until the computation fully converges to a satisfactory solution. As proved here, the deviation of the 1-1/2-D solution from the 1-D solution is a powerful tool for investigation of instability of a flux function.

2. *Shock Locations That are Unstable in One Dimension*

According to Table 2, all of the cases that were unstable in 1-D were, with few exceptions, unstable in 1-1/2-D. This even includes the cases of AUSMPW+ and RoeM2 that feature multidimensional dissipation. In Fig. 10, we present the results of these schemes for cases that were unstable in 1-D. It seems that in the case of AUSMPW+ ($\varepsilon = 0.9$), the dissipation is able to suppress both the 1-D and the multidimensional modes. In the case of RoeM2 ($\varepsilon = 0.0$), however, the 1-D mode remains, though not for the $\varepsilon = 0.7$ and 0.8 cases. RoeM2 without the multidimensional dissipation ($\varepsilon = 0.0$) is one of the few exceptions. As shown before, however, this version of the RoeM2 scheme failed this test for another choice of shock location. Thus, by eliminating the multidimensional dissipation, the scheme just changed its favorite shock location. The HLLE scheme, because of its inability to sustain contact discontinuities, has a built-in dissipation that also completely suppresses the additional modes but leaves the 1-D mode in place. Thus, HLLE is not carbuncle-free, although it has been believed to be so.

Table 2 Summary of computed results for 1-D and the 1-1/2-D $M_0 = 6.0$ steady shock with various schemes (S: symmetry and converged, A: asymmetry and converged, U: not converged)

Scheme	Test problem	$\varepsilon = 0.0$	0.1	0.2	0.3	0.4	0.5	0.6	0.7	0.8	0.9
Godunov	1-D	U	S	S	S	S	S	S	U	U	U
	1-1/2-D	U	U	U	U	U	U	U	U	U	U
Roe	1-D	U	S	S	S	S	S	S	U	U	U
	1-1/2-D	U	S	S	S	U	U	U	U	U	U
Roe (E-fix)	1-D	S	S	S	S	S	S	S	S	S	S
	1-1/2-D	U	U	U	U	U	U	U	U	U	U
EC-Roe ($\alpha = 0.2$)	1-D	S	S	S	S	S	U	U	U	U	S
	1-1/2-D	S	S	S	U	U	S	U	U	U	S
EC-Roe ($\alpha = 0.8$)	1-D	S	S	S	S	S	S	S	S	S	S
	1-1/2-D	U	U	U	U	U	U	U	U	U	U
AUSM+	1-D	S	S	S	S	U	U	S	S	S	S
	1-1/2-D	S	S	S	S	U	U	U	U	S	S
AUSM$^+$-up	1-D	S	S	S	S	S	U	U	U	S	S
	1-1/2-D	S	S	S	S	S	A	U	U	U	S
AUSMPW+	1-D	S	S	S	S	S	S	S	U	U	U
	1-1/2-D	S	S	S	S	S	S	S	U	U	S
(without multidimensional term)	1-1/2-D	U	S	S	S	S	A	U	U	U	U
RoeM2	1-D	U	S	S	S	S	S	S	S	U	U
	1-1/2-D	U	A	A	A	A	S	A	U	U	U
(without multidimensional term)	1-1/2-D	S	S	S	S	S	A	A	S	S	S
HLLE	1-D	U	S	S	S	S	S	S	U	U	U
	1-1/2-D	U	S	S	S	S	S	S	U	U	U

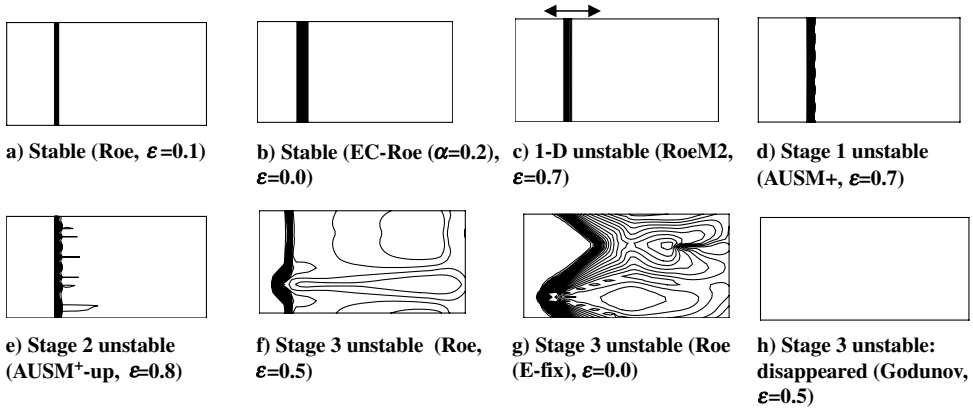

a) Stable (Roe, ε=0.1) b) Stable (EC-Roe (α=0.2), ε=0.0) c) 1-D unstable (RoeM2, ε=0.7) d) Stage 1 unstable (AUSM+, ε=0.7)

e) Stage 2 unstable (AUSM$^+$-up, ε=0.8) f) Stage 3 unstable (Roe, ε=0.5) g) Stage 3 unstable (Roe (E-fix), ε=0.0) h) Stage 3 unstable: disappeared (Godunov, ε=0.5)

Fig. 5 Typical examples of Mach number contours at 40,000 time steps for the 1-1/2-dimensional steady shock (freestream Mach number $M_0 = 6.0$ and shock position ε is one-dimensionally stable).

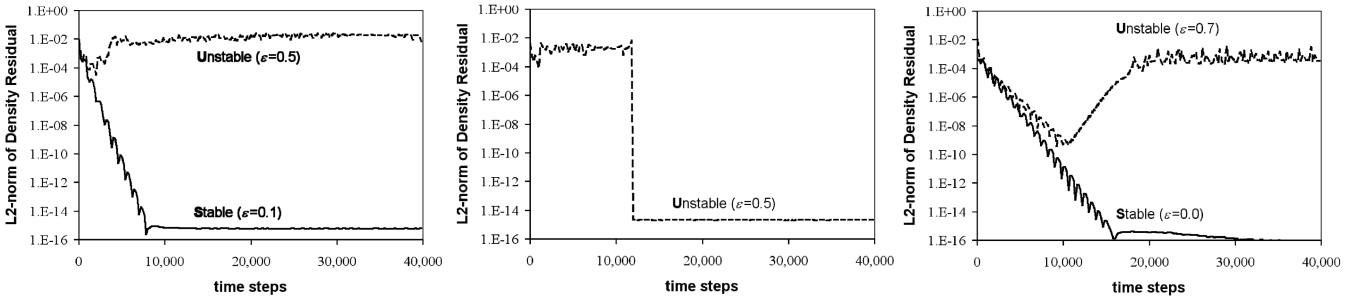

a) Roe, stable (ε=0.1) and unstable b) Godunov, unsatble: disappeared (ε=0.5) c) AUSM+, stable (ε=0.0) and unstable (ε=0.7)

Fig. 6 Residual histories for 1-1/2-dimensional steady shock (freestream Mach number $M_0 = 6.0$ and shock position ε is one-dimensionally stable).

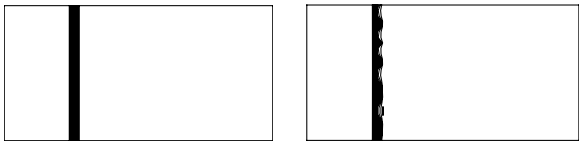

a) b)

Fig. 7 Mach number contours at a) 10,000 and b) 20,000 time steps for the 1-1/2-dimensional steady shock (AUSM+, freestream Mach number $M_0 = 6.0$ and shock position $\varepsilon = 0.7$).

We confirmed our expectation that if a scheme is unstable in 1-D, then it remains unstable in 1-1/2-D even if a multidimensional dissipation is added. This suggests that the scheme of Sanders et al. [23] would also be unstable in 1-1/2-D for certain cases, although we have not confirmed this by experiment.

In summary, we have found 1-D stable schemes [EC-Roe scheme ($\alpha = 0.8$) and Roe (E-fix)] but no 1-1/2-D stable schemes. The following schemes are stable only under certain shock locations: Roe, EC-Roe ($\alpha = 0.2$), AUSM+, AUSM$^+$-up, AUSMPW+ (with and without multidimensional dissipation), RoeM2 (with and without multidimensional dissipation), and HLLE.

A natural question arises here: What if a 1-D stable scheme is equipped with a multidimensional dissipation? One example to answer this is found in our latest work [24], in which an anomalous result of EC-Roe ($\alpha = 0.8$) is greatly (not perfectly, though) improved with a surface-tension-like multidimensional dissipation that is applicable to unstructured grids. Thus, it is said that such a combination is very promising for development of a carbuncle-free scheme in a strong sense. This result supports our claim that 1-D and multidimensional dissipations should be separately considered.

In addition, we leave a few comments on very recent results in [18,19]. It was reported therein that a combination of Roe (E-fix) and HLLE (called a "rotated-RHLL" flux) successfully passed all the 1-1/2-D tests, as well as van Leer type of flux-vector-splitting schemes [25,26], on the limitation of the present criterion. We do not pursue those results in the present work, but these fluxes are, according to the discussions here, likely to produce the proper amount of dissipations in both the normal and parallel directions to the shock.

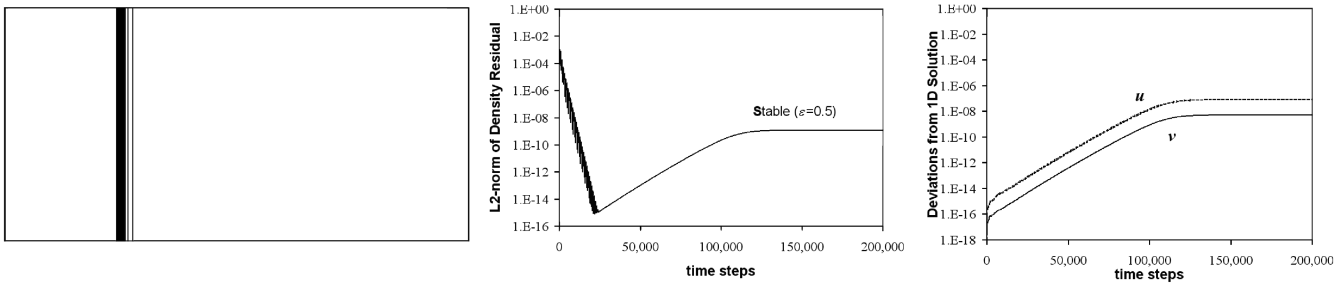

a) b) c)

Fig. 8 Plots of a) Mach number contours at 200,000 time steps, b) residual histories, and c) histories of deviations of primitive variables from 1-D solutions for the 1-1/2-dimensional steady shock (RoeM2, freestream Mach number $M_0 = 6.0$ and shock position $\varepsilon = 0.5$).

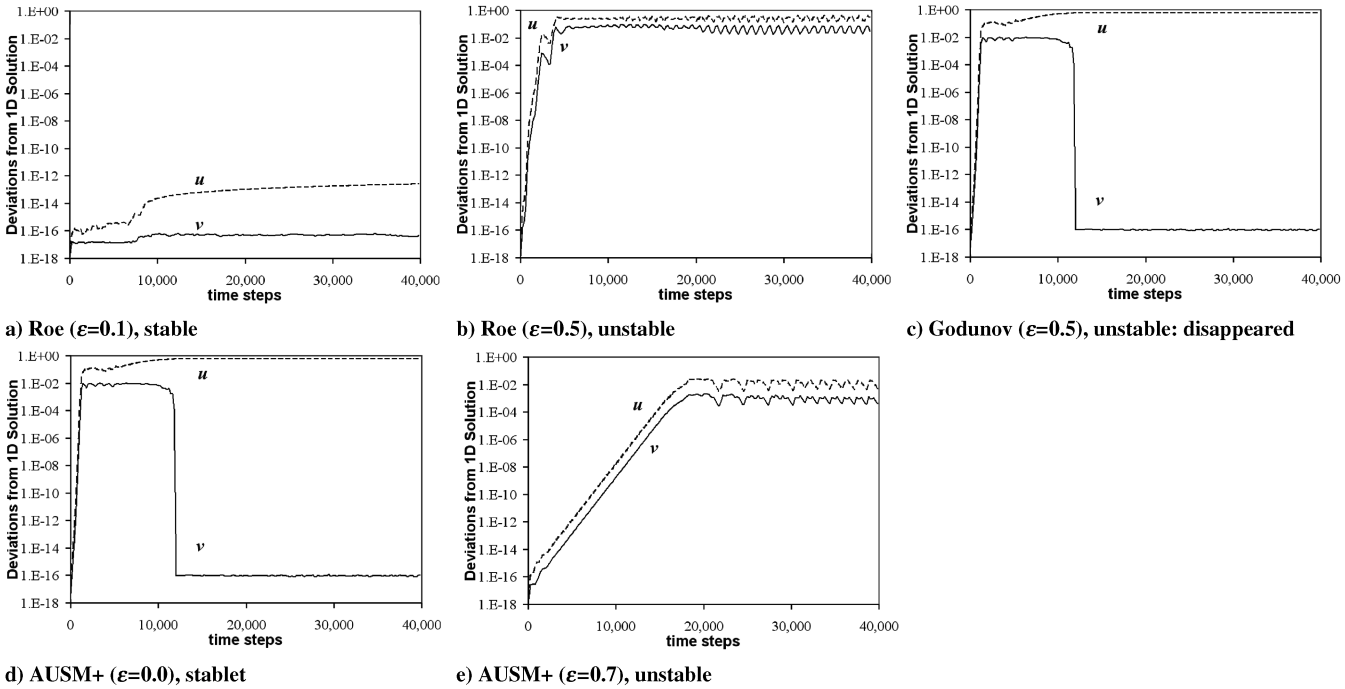

a) Roe (ε=0.1), stable

b) Roe (ε=0.5), unstable

c) Godunov (ε=0.5), unstable: disappeared

d) AUSM+ (ε=0.0), stablet

e) AUSM+ (ε=0.7), unstable

Fig. 9 Histories of deviations of primitive variables from 1-D solutions (freestream Mach number $M_0 = 6.0$ and shock position ε is one-dimensionally stable).

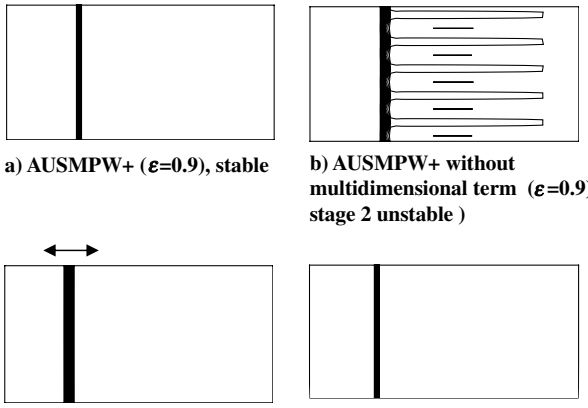

a) AUSMPW+ (ε=0.9), stable

b) AUSMPW+ without multidimensional term (ε=0.9), stage 2 unstable)

c) RoeM2 (ε=0.0), 1-D unstable

d) RoeM2 without multidimensional term (ε=0.0), stable

Fig. 10 Effects of multidimensional terms in AUSMPW+ and RoeM2: Mach number contours at 40,000 time steps for the 1-1/2-dimensional steady shock (freestream Mach number $M_0 = 6.0$ and shock position ε is one-dimensionally unstable).

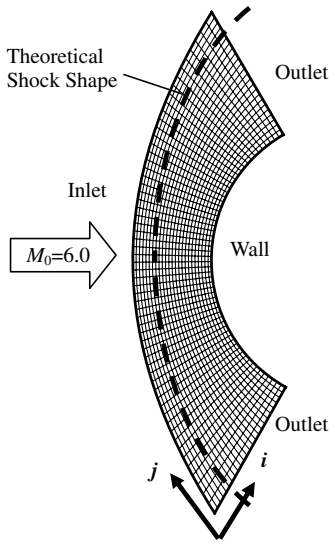

Fig. 11 Computational grid and conditions for the blunt-body problem.

C. Two-Dimensional Problem: Hypersonic Flow over a Blunt Body with a Shock-Aligned Grid

Finally, we will go on to a fully 2-D problem. Figure 11 shows the computational grid and conditions in this case. The grid has 48×120 cells and has initially been designed so that a fitted bow shock lies on an $i = \text{const}$ line for $M_0 = 6.0$.** We checked that our version of this grid was perfectly symmetric by removing some very small rounding errors that arose due to translation from the format in which the grid was received. We then stretched this grid outward, controlling the motion of the $i = \text{const}$ line that theoretically coincides with the shock position. We introduced a parameter δ such that if $\delta = 0$, we recover the original grid, but if $\delta = 1$, the adjacent grid line moves to the theoretical shock location. We varied this parameter by intervals of $1/8$ so that, just as in the earlier tests, the shock took up a variety of locations relative to the grid line. We expected that if our results were stable for $\delta = 0$, they were also stable for $\delta = 1$. However, there were a few exceptions, perhaps because the captured shocks were not exactly aligned with the grid. As the parameter δ changes by unity, so does the parameter ε, but they are not the same because the captured shocks will not be in exactly the same position as the fitted shock.

The specified condition at the inlet ($i = 0$) is just the freestream Mach number of $M_0 = 6.0$ with reference density and pressure. The slip condition is applied at the wall ($i = i_{\max} + 1$), and the simple extrapolation is employed at the outlet ($j = 0$ and $j_{\max} + 1$). Computations were conducted with CFL $= 0.5$ for 50,000 time steps unless the residual converged to machine zero. The spatial accuracy is first order or second order by using the MUSCL scheme [27] with van Albada's limiter [28].

Two examples of computed flowfields are shown in Fig. 12. Compared here are results of the second-order Roe scheme with $\delta = 0$ (no displacement) and $\delta = 4/8$ (half-cell displacement). The bow shock exactly lies on an $i = \text{const}$ line and the solution converged successfully for $\delta = 0$; however, for $\delta = 4/8$, the shock

**Private communication with Jeffery White et al. NASA Langley Research Center, Apr. 2007.

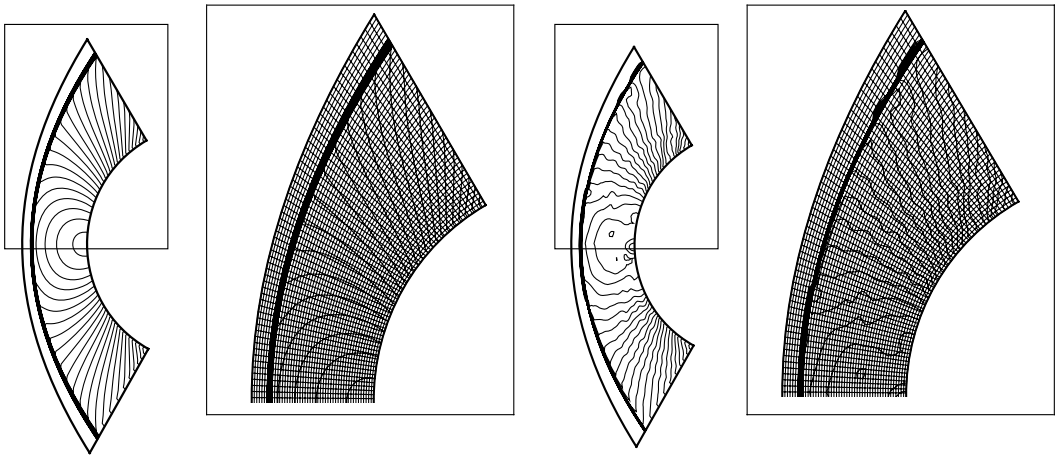

a) δ=0 b) δ=4/8

Fig. 12 Pressure contours with grid around 2-D cylinder at 50,000 time steps (Roe, second order).

seemed to look for a comfortable position rather than settle down on a particular $i = \text{const}$ line, and the solution did not converge. This observation is similar to that shown in the previous test cases.

In Table 3 we summarized the results for various flux functions investigated in the preceding subsections. Computed flowfields selected from each scheme are shown in Fig. 13. According to these results, the following discussions have been drawn:

1) All the schemes presented here showed unstable (U) or asymmetric (A) results for some conditions. In every case, we find some set of consecutive positions for which the solution is stable (S) and another set for which it is unstable (U). Sometimes these sets are separated by an example of case A. This behavior was also noted in the 1-D and 1-1/2-D tests.

2) The shock locations for stable and unstable are different for different schemes, again, as in the 1-D and 1-1/2-D tests.

3) These shock locations are also different for different orders of spatial accuracies (e.g., the EC-Roe scheme with $\alpha = 0.2$ favors $3/8 \le \delta \le 6/8$ for first order and $4/8 \le \delta \le 7/8$ for second order). This difference would be due to the difference of computed shock standoff distances.

4) The entropy fix slightly helped the Roe scheme to be stable for second-order, but not for first-order, computations.

5) The EC-Roe scheme with $\alpha = 0.8$ failed all the cases, in contrast to 1-D tests, but as in 1-1/2-D cases. The effect of adding dissipation is seen from Figs. 13d and 13e by comparing the thickness of the captured shocks. If too much dissipation is added on a flux function (and the shock is broadened), the flux function seems more likely to be vulnerable to the multidimensional shock instability, as mentioned in the 1-1/2-D tests.

6) Schemes equipped with multidimensional effects (AUSMPW+ and RoeM2) still suffered from shock instability, although they worked well for limited cases.

7) Schemes that are claimed to be carbuncle-free, including HLLE, are not actually shock stable.

These results are broadly similar to the 1-1/2-D results. For most of the schemes, the proportions of stable and unstable cases were about the same. Again, there is no stable scheme.

An extension of the present discussions to 3-D viscous problems appears in [19], in which further degrees of freedom trigger the multidimensional instability.

Table 3 Summary of computed results for the $M_0 = 6.0$ 2-D cylinder with various schemes (S: symmetry and converged, A: asymmetry and converged, and U: not converged)

Scheme	Order of accuracy	$\delta = 0$	1/8	2/8	3/8	4/8	5/8	6/8	7/8	1
Godunov	First	A	A	A	U	U	S	S	S	S
	Second	S	S	U	A	U	U	S	S	S
Roe	First	A	A	A	U	U	A	A	A	U
	Second	S	U	U	U	U	U	S	S	S
Roe (E-fix)	First	A	A	A	A	A	A	A	A	A
	Second	S	S	U	U	U	U	S	S	S
EC-Roe ($\alpha = 0.2$)	First	U	U	A	S	S	S	S	A	U
	Second	U	U	U	U	S	S	S	S	U
EC-Roe ($\alpha = 0.8$)	First	U	A	A	U	U	U	A	U	U
	Second	U	U	U	U	U	U	U	U	U
AUSM+	First	U	U	U	S	S	S	S	A	U
	Second	S	S	U	U	S	U	U	U	U
AUSM$^+$-up	First	U	U	U	S	S	S	S	A	U
	Second	S	S	U	U	S	U	U	U	U
AUSMPW+	First	S	S	S	S	S	S	U	S	S
	Second	S	S	S	U	U	S	S	S	S
(without multidimensional term)	First	S	S	S	A	U	A	U	S	S
	Second	S	S	S	U	U	S	S	S	S
RoeM2	First	S	S	S	A	U	S	S	S	S
	Second	S	S	S	S	U	U	S	S	S
(without multidimensional term)	First	S	S	S	U	U	S	S	S	S
	Second	S	S	U	U	U	U	S	S	S
HLLE	First	S	S	S	U	U	S	S	S	S
	Second	S	S	S	U	U	U	S	S	S

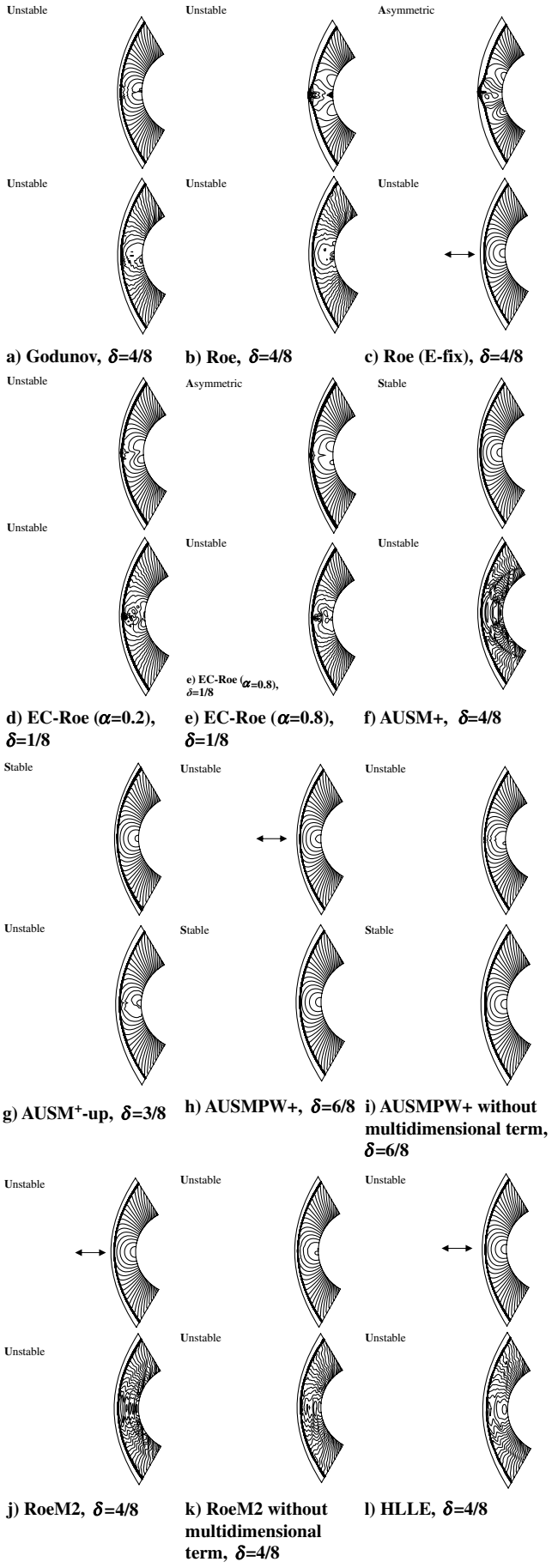

Fig. 13 Typical examples of pressure at 50,000 time steps; first order (upper) and second order (lower) around the 2-D cylinder.

IV. Conclusions

We have conducted a broad range of investigations of hypersonic shock stability within the common framework of upwind shock-capturing schemes. We have focused on the role played by the relative positioning of the shock on the grid.

1) There are at least two kinds of shock instabilities: one is one-dimensional (1-D) and the other is multidimensional.

2) All but two of the flux functions investigated were unstable, even in 1-D, for at least some combinations of shock location and freestream Mach number. The exceptions, Roe with entropy fix and EC-Roe ($\alpha = 0.8$), satisfy the second law of thermodynamics (i.e., proper entropy creation across the shock).

3) All the fluxes, including those two fluxes, showed unstable results in multidimensional (1-1/2-D and 2-D) tests. Thus, we think it likely that some form of multidimensional dissipation is required. On the limited basis of the present tests, the dissipation in the context of AUSMPW+ [5] seems more reliable than that for RoeM2 [6]. However, they are effective only when the multidimensional instability standalone is present; they do not work well if 1-D mode also appears at the same time. Moreover, neither is formulated for use on unstructured grids.

Acknowledgments

This work was carried out at the University of Michigan, Ann Arbor, MI, when the first author was studying there as an exchange student from Nagoya University, Japan. He is grateful to Bram van Leer (University of Michigan); Yoshiaki Nakamura, Tsutomu Nomizu, and the International Academic Exchange Office (Nagoya University) for their relevant support. This work was partly supported by the Japan Aerospace Exploration Agency's Engineering Digital Innovation (JEDI) center (managed by Eiji Shima), Yoshiaki Nakamura and his colleagues (Nagoya University), and Ken Powell (University of Michigan). Jeffery White and his colleagues (NASA Langley Research Center) supplied us with a computational grid for a Mach 6 blunt-body problem. Tomoyuki Hanawa (Chiba University, Japan), Hiroaki Nishikawa (National Institute of Aerospace), Akihiro Sasoh and Katsuya Ishii (Nagoya University), and colleagues of the first author at the JEDI center gave us constructive comments. We thank them all for their cooperation.

References

[1] Peery, K. M., and Imlay, S. T., "Blunt-Body Flow Simulations," AIAA Paper 88-2904, 1988.

[2] Pandolfi, M., and DfAmbrosio, D., "Numerical Instabilities in Upwind Methods: Analysis and Cures for the Carbuncle Phenomenon," *Journal of Computational Physics*, Vol. 166, No. 2, 2001, pp. 271–301. doi:10.1006/jcph.2000.6652

[3] Barth, T. J., "Some Notes on Shock-Resolving Flux Functions Part 1: Stationary Characteristics," NASA TM-101087, 1989.

[4] Godunov, S. K., "A Finite Difference Method for the Numerical Computation of Discontinuous Solutions of the Equations of Fluid Dynamics," *Matematicheskii Sbornik/Izdavaemyi Moskovskim Matematicheskim Obshchestvom*, Vol. 47, No. 3, 1959, pp. 271–306.

[5] Roe, P. L., "Approximate Riemann Solvers, Parameter Vectors, and Difference Schemes," *Journal of Computational Physics*, Vol. 43, No. 2, 1981, pp. 357–372. doi:10.1016/0021-9991(81)90128-5

[6] Liou, M. S., "A Sequel to AUSM: AUSM+," *Journal of Computational Physics*, Vol. 129, No. 2, 1996, pp. 364–382. doi:10.1006/jcph.1996.0256

[7] Liou, M. S., "A Further Development of the AUSM+ Scheme Towards Robust and Accurate Solutions for All Speeds," AIAA Paper 2003-4116, 2003.

[8] Kim, K. H., Kim, C., and Rho, O. H., "Methods for the Accurate Computations of Hypersonic Flows 1: AUSMPW+ Scheme," *Journal of Computational Physics*, Vol. 174, No. 1, 2001, pp. 38–80. doi:10.1006/jcph.2001.6873

[9] Kim, S. S., Kim, C., Rho, O. H., Hong, S. K., "Cures for the Shock Instability: Development of a Shock-Stable Roe Scheme," *Journal of Computational Physics*, Vol. 185, No. 2, 2003, pp. 342–374. doi:10.1016/S0021-9991(02)00037-2

[10] Einfeldt, B., "On Godunov-Type Methods for Gas Dynamics," *SIAM Journal on Numerical Analysis*, Vol. 25, No. 2, 1988, pp. 294–318. doi:10.1137/0725021

[11] Ismail, F., "Toward a Reliable Prediction of Shocks in Hypersonic Flow —Resolving Carbuncles with Entropy and Vorticity Control," Ph.D. Dissertation, Univ. of Michigan, Ann Arbor, MI, 2006.

[12] Ismail, F., Roe, P. L., and Nishikawa, H., "A Proposed Cure to the Carbuncle Phenomenon," The Fourth International Conference on Computational Fluid Dynamics, Paper U18, 2006.

[13] Roe, P. L., "Affordable, Entropy-Consistent, Euler Flux Functions 1: Analytical Results," *Journal of Computational Physics* (submitted for publication).

[14] Ismail, F., and Roe, P. L., "Affordable, Entropy-Consistent, Euler Flux Functions 2: Entropy Production at Shocks," *Journal of Computational Physics* (to be published).

[15] Roe, P. L., "Fluctuations and Signals—A Framework for Numerical Evolution Problems," *Numerical Methods for Fluid Dynamics*, edited by K. W. Morton, and M. J. Baines, Academic Press, New York, 1982, pp. 219–257.

[16] Chauvat, Y., Moschetta, J. M., and Gressier, J., "Shock Wave Numerical Structure and the Carbuncle Phenomenon," *International Journal for Numerical Methods in Fluids*, Vol. 47, Nos. 8–9, 2005, pp. 903–909. doi:10.1002/fld.916

[17] Harten, A., "High Resolution Schemes for Hyperbolic Conservation Laws," *Journal of Computational Physics*, Vol. 49, No. 3, 1983, pp. 357–393. doi:10.1016/0021-9991(83)90136-5

[18] Nishikawa, H., and Kitamura, K., "Very Simple, Carbuncle-Free, Boundary-Layer-Resolving, Rotated-Hybrid Riemann Solvers," *Journal of Computational Physics*, Vol. 227, No. 4, 2008, pp. 2560–2581. doi:10.1016/j.jcp.2007.11.003

[19] Kitamura, K., Nakamura, Y., and Shima, E., "An Evaluation of Euler Fluxes 2: Hypersonic Surface Heating Computation," 38th AIAA Fluid Dynamics Conference and Exhibit, Seattle, WA, AIAA Paper 2008-4275, 2008.

[20] Quirk, J. J., "A Contribution to the Great Rimann Solver Debate," *International Journal for Numerical Methods in Fluids*, Vol. 18, No. 6, 1994, pp. 555–574. doi:10.1002/fld.1650180603

[21] Dumbser, M., Moschetta, J. M., and Gressier, J., "A Matrix Stability Analysis of the Carbuncle Phenomenon," *Journal of Computational Physics*, Vol. 197, No. 2, 2004, pp. 647–670. doi:10.1016/j.jcp.2003.12.013

[22] Roe, P. L., Nishikawa, H., Ismail, F., and Scalabrin, L., "On Carbuncles and Other Excrescences," AIAA Paper 2005-4872, 2005.

[23] Sanders, R., Morano, E., and Druguetz, M. C., "Multidimensional Dissipation for Upwind Schemes: Stability and Applications to Gas Dynamics," *Journal of Computational Physics*, Vol. 145, No. 2, 1998, pp. 511–537. doi:10.1006/jcph.1998.6047

[24] Roe, P. L., and Kitamura, K., "Artificial Surface Tension to Stabilize Captured Shockwaves," 38th AIAA Fluid Dynamics Conference and Exhibit, Seattle, WA, AIAA Paper 2008-3991, 2008.

[25] van Leer, B., *Flux Vector Splitting for the Euler Equations*, *Eighth International Conference of Numerical Methods in Fluid Dynamics*, Lecture Notes in Physics, Vol. 170, Springer, Berlin, 1982, pp. 507–512.

[26] Hänel, D., Schwane, R., and Seider, G., "On the Accuracy of Upwind Schemes for the Solution of the Navier-Stokes Equations," AIAA Paper 87-1105, 1987.

[27] van Leer, B., "Towards the Ultimate Conservative Difference Scheme 5: A Second-Order Sequel to Godunov's Method," *Journal of Computational Physics*, Vol. 32, No. 1, 1979, pp. 101–136. doi:10.1016/0021-9991(79)90145-1

[28] van Albada, G. D., van Leer, B., and Roberts, W. W. Jr., "A Comparative Study of Computational Methods in Cosmic Gas Dynamics," *Astronomy and Astrophysics*, Vol. 108, No. 1, 1982, pp. 76–84.

Z. Wang
Associate Editor